






**Magnetic phase transitions in the antiferromagnet  $\text{CuB}_2\text{O}_4$  optically detected via Frenkel excitons**D. Kudlacik <sup>1</sup>, N. E. Kopteva <sup>1</sup>, D. R. Yakovlev <sup>1,2</sup>, M. Bayer <sup>1</sup> and R. V. Pisarev <sup>2</sup><sup>1</sup>*Experimentelle Physik 2, Technische Universität Dortmund, 44221 Dortmund, Germany*<sup>2</sup>*Ioffe Institute, Russian Academy of Sciences, 194021 St. Petersburg, Russia*

(Received 26 April 2024; accepted 26 July 2024; published 5 August 2024)

The copper metaborate  $\text{CuB}_2\text{O}_4$  with a unique noncentrosymmetric crystal structure and the two structurally nonequivalent  $4b$  and  $8d$  magnetic subsystems of  $\text{Cu}^{2+}$  ions are characterized by several commensurate and incommensurate magnetic phases below the Néel temperature of  $T_N = 20$  K. Transitions between them can be induced by varying the sample temperature or the applied magnetic field. High-resolution optical spectroscopy of the Frenkel exciton states is used to probe the magnetic phase transitions. The absorption spectra are measured in the temperature range from 4.3 K up to  $T_N$  and in magnetic fields up to 2 T. The exciton transitions are observed in the range of 1.405–1.407 eV and are related to the lowest-energy electronic transition in the  $4b$  magnetic subsystem of  $\text{Cu}^{2+}$  ions, thus allowing us to monitor the behavior of this particular subsystem. The exciton lines show abrupt changes of intensity and energy splitting, which can be unambiguously attributed to the magnetic phase transitions in the  $4b$  subsystem. The magnetic phase diagram reconstructed from the spectroscopic experiments on the  $4b$  subsystem is compared with those from magnetic measurements, which reflect the magnetic behavior of both the  $4b$  and  $8d$  subsystems. The suggested spectroscopic approach enables separate monitoring of the temperature and magnetic field behavior of different magnetic subsystems in structurally and magnetically complex compounds.

DOI: [10.1103/PhysRevB.110.054408](https://doi.org/10.1103/PhysRevB.110.054408)**I. INTRODUCTION**

The fundamental study of multiferroic and magnetoelectric materials, which are typically characterized by complex magnetic structures and interactions between different magnetic and nonmagnetic subsystems, has raised a lot of interest during the past two decades due to the possibility of switching their physical properties under an external influence. Many studies have shown that besides interesting physical phenomena observed in these materials, they also provide a solid platform for applications [1–11].

Among the wide variety of multiferroic and magnetoelectric materials, the copper metaborate ( $\text{CuB}_2\text{O}_4$ ) generates considerable excitement due to its magnetic, optical, magneto-optical, and nonlinear optical properties. Below the Néel temperature of  $T_N = 20$  K,  $\text{CuB}_2\text{O}_4$  is a Heisenberg-type antiferromagnet that has several commensurate and incommensurate magnetic phases. The first study of these phases and the phase diagram of  $\text{CuB}_2\text{O}_4$  has been worked out by magnetic susceptibility and magnetization measurements [12]. This was followed by applying a variety of experimental methods for comprehensive investigations of the magnetic properties of  $\text{CuB}_2\text{O}_4$  and its successive phase transitions, such as the measurement of high-field electron spin resonance [13], neutron diffraction [14–16], magnetization [17], and thermal conductivity [18]. High-resolution linear and nonlinear optical spectroscopy, such as sublattice-sensitive magnetic linear dichroism (MLD) [19], Fourier spectroscopy [20], and magnetic-field-induced second harmonic generation (SHG) [21–23] were also used to address the magnetic and optical properties of  $\text{CuB}_2\text{O}_4$  and to detect transitions between the magnetic phases [24].

The optical properties of  $\text{CuB}_2\text{O}_4$  in the near infrared, visible, and ultraviolet spectral range are controlled by absorption of and emission from the electronic transitions within the  $\text{Cu}^{2+}$  ions [21]. These ions occupy the two crystallographically nonequivalent  $4b$  and  $8d$  positions, forming two magnetic subsystems that contribute very differently to the magnetic and optical properties. Details on  $\text{CuB}_2\text{O}_4$  crystal cells can be found in Refs. [15,25]. It should be noted that most of the studies carried out to date on the optical phenomena in copper metaborate have focused primarily on the  $4b$  subsystem, although studies of the  $8d$  subsystem are also of great interest.

The efficient photoluminescence [26] and the magnetic-field-induced directional photoluminescence [27] related to the lowest in energy electronic transition in the  $4b$  subsystem are surprising observations for  $\text{CuB}_2\text{O}_4$ . The material is also an excellent platform for the study of nonlinear optical phenomena, such as SHG [21–23], the giant optical magnetoelectric effect [28], one-way light transparency [29], and for the analysis of optical nonreciprocity phenomena [30,31]. A huge nonreciprocity has been observed for the magnetic-field-induced SHG on the lowest-energy electronic transition [22,23]. Light absorption at this transition gives rise to observation of the Davydov splitting of the Frenkel exciton and allows study of the spin properties of the Frenkel excitons in strong magnetic fields [32]. Theoretical calculations show that the doublet structure of the Frenkel exciton in weak magnetic fields is determined by the exchange interactions between the  $\text{Cu}^{2+}$  spins. Therefore, the Frenkel exciton can be used as a probe for optical detection of the magnetic interactions in  $\text{CuB}_2\text{O}_4$ , which we explore in this paper.

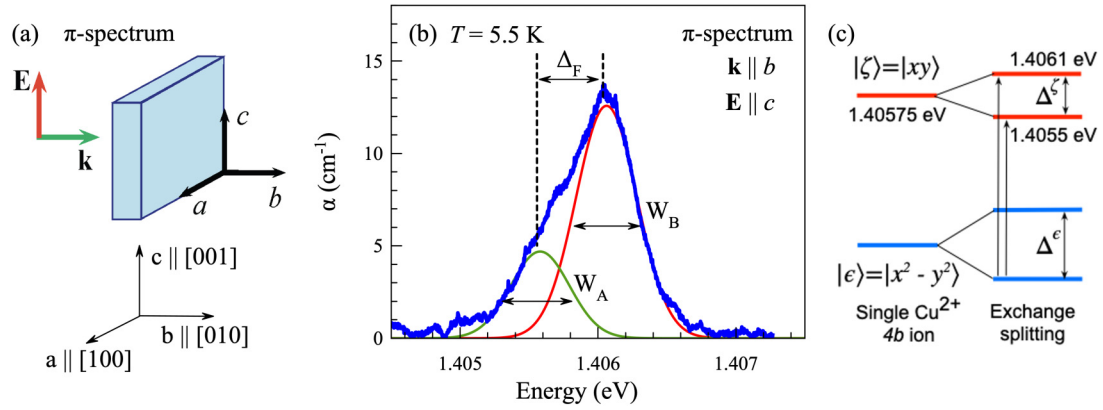


FIG. 1. (a) Scheme of the sample axes orientation relative to the light  $k$  vector and the light polarization vector  $\mathbf{E}$ . The geometry  $\mathbf{E} \parallel c$  and  $\mathbf{k} \parallel b$  is used for measuring the absorption  $\pi$  spectrum. (b) Absorption  $\pi$  spectrum of  $\text{CuB}_2\text{O}_4$  (blue line) measured at  $T = 5.5$  K in the spectral range of the lowest photon-energy transition from the ground  $|\epsilon\rangle = |x^2 - y^2\rangle$  state to the lowest-in-energy  $|\zeta\rangle = |xy\rangle$  excited state of the  $\text{Cu}^{2+}$  ions in the  $4b$  magnetic subsystem. Green and red lines show the deconvolution of the spectrum into the two states of the Frenkel excitons split by  $\Delta_F = \Delta^\zeta$  with FWHMs denoted by  $W_{A(B)}$ . (c) Energy level diagram of the ground  $|\epsilon\rangle = |x^2 - y^2\rangle$  and excited  $|\zeta\rangle = |xy\rangle$  state of a single  $\text{Cu}^{2+}$  ion. The exchange interaction between neighboring  $\text{Cu}^{2+}$  ions in the  $4b$  and  $8d$  subsystems splits the ground and excited states of the  $4b$   $\text{Cu}^{2+}$  ions by  $\Delta^\epsilon$  and  $\Delta^\zeta$ , respectively [32].

In this paper we use the Frenkel excitons as optical probes to address and distinguish magnetic phases in antiferromagnetic  $\text{CuB}_2\text{O}_4$ . The experimental study focuses on the Frenkel excitons in the 1.405–1.407 eV spectral range of the electronic transitions in the  $4b$  subsystem of  $\text{Cu}^{2+}$  ions. It is carried out in the temperature range from 4.3 K up to the  $T_N$  and in magnetic fields up to 2 T. We reconstruct through the optical experiments the magnetic field–temperature phase diagram for the magnetic field applied along and perpendicular to the tetragonal  $c$  axis. This diagram is compared with the one obtained from magnetic susceptibility data of Ref. [17].

## II. SAMPLES AND EXPERIMENTAL DETAILS

We studied a sample prepared from a single crystal of  $\text{CuB}_2\text{O}_4$  grown by the Kyropoulos technique using a melt of  $\text{B}_2\text{O}_3$ ,  $\text{CuO}$ ,  $\text{Li}_2\text{O}$ , and  $\text{MoO}_3$  oxides [33]. A (101) plate with a thickness of 1.12 mm is cut from the single crystal and oriented using Laue x-ray diffraction patterns, so that the  $c$  axis is parallel to the [001] direction and the  $a$  axis is parallel to the [100] direction, both axes being in the plane of the sample. A schematic of the sample orientation is shown in Fig. 1(a). For the absorption measurements, we use a halogen lamp with low excitation density of  $0.5 \text{ mW/cm}^2$ . Linear polarization of the light is set by a Glan-Thompson prism and rotated by a  $\lambda/2$  retardation plate. In this study, only the  $\pi$  spectrum is measured, where the light polarization  $\mathbf{E}$  is oriented along the  $c$  axis and the light  $k$  vector is oriented along the  $b$  axis. This choice of polarization is made to avoid absorption saturation in the thick sample. The absorption properties of  $\text{CuB}_2\text{O}_4$  are described in detail in Refs. [21,22,26,32].

The sample is mounted strain-free in a helium bath cryostat with a split-coil solenoid. The temperature can be varied from 4.3 up to  $T_N$  and the magnetic field can be changed from zero to 2 T. The magnetic field ( $\mathbf{B}$ ) is oriented perpendicular to the light  $k$  vector and is applied in the two geometries  $\mathbf{B}_a \parallel a$  and  $\mathbf{B}_c \parallel c$ . To achieve this, the sample is rotated in the  $ac$  plane by  $90^\circ$ . The light transmitted through the sample

is dispersed by a triple-spectrometer (Princeton Instruments TriVista TR555) with a total focal length of 1.5 m, which consists of three 0.5 m single spectrometers. The signal is detected by a silicon charge-coupled device (CCD) camera with  $512 \times 2048$  pixels of  $13.5 \mu\text{m}$  size, providing a spectral resolution of about  $30 \mu\text{eV}$ .

## III. EXPERIMENTAL RESULTS AND DISCUSSION

The absorption spectra of  $\text{CuB}_2\text{O}_4$  in the 1.4–2.5 eV spectral range exhibit numerous zero-phonon lines that arise from  $d-d$  optical transitions in the  $4b$  and  $8d$  subsystems of the  $\text{Cu}^{2+}$  ions [21]. In this paper we specifically examine the lowest energy transition in the  $4b$  subsystem.

### A. Optical detection of magnetic phase transitions via Frenkel excitons

Figure 1(b) shows the absorption  $\pi$  spectrum of the  $\text{Cu}^{2+}$  ions in the  $4b$  subsystem measured at  $T = 5.5$  K within the spectral range of 1.405–1.407 eV. The spectrum is composed of two lines, the decomposition of which using Gaussian peaks is shown by the red and green lines. We refer to the lower energy line at 1.4055 eV as line A and to the higher energy line at 1.4061 eV as line B [32]. Their absorption coefficients are  $\alpha_A = 4.7 \text{ cm}^{-1}$  and  $\alpha_B = 12.6 \text{ cm}^{-1}$ , giving the ratio of  $\alpha_B/\alpha_A = 2.68$ . Note that this choice of the light  $\pi$  polarization corresponds to magnetic dipole transitions and the observed absorption values are much lower than those for  $\sigma$  polarization for which values of  $150 \text{ cm}^{-1}$  can be reached [21].

The energy difference between the two lines in Fig. 1(b) amounts to  $\Delta_F = 0.57 \text{ meV}$  at 5.5 K with similar full widths at half maximum (FWHM) of  $W_A = 0.48 \text{ meV}$  and  $W_B = 0.44 \text{ meV}$ . Note that these values are subject to slight changes with temperature and magnetic phase at zero field. The light is absorbed by Frenkel excitons, associated with the optical transition between the ground state  $|\epsilon\rangle = |x^2 - y^2\rangle$  and the

excited state  $|\zeta\rangle = |xy\rangle$  of the  $\text{Cu}^{2+}$  ions at the  $4b$  sites. The exchange interaction between the copper ions leads to a splitting of the ground and excited states by  $\Delta^\epsilon$  and  $\Delta^\zeta$ , respectively, as shown in Fig. 1(c). In the antiferromagnetic phase below  $T_N$ , the ground state is split due to the exchange field caused by the neighboring copper spins. This splitting is approximately 7.2 meV [27]. Therefore, it is assumed that, at low temperatures, only the lower  $m_s = -1/2$  substate of the spin doublet is populated. The optical transitions from the lower ground state to the two excited states create the doublet structure of the Frenkel exciton [32]. Therefore, the splitting  $\Delta_F(0 \text{ T}) = \Delta^\zeta$  provides a direct measure of the exchange interaction between the  $\text{Cu}^{2+}$  spins in the excited state and it strongly depends on the spin structure of the  $4b$  subsystem.

The  $4b$  subsystem consists of the four copper spins in the unit cell ( $\mathbf{S}_\alpha, \mathbf{S}_\beta, \mathbf{S}_\gamma, \mathbf{S}_\delta$ ). At equilibrium in zero magnetic field, the spins in a single domain antiferromagnetic state are oriented along the [110] easy axis in the commensurate antiferromagnetic phase. It is convenient to describe the joint orientation of the four spins by using the ferromagnetic  $\mathbf{M} = \mathbf{S}_\alpha + \mathbf{S}_\beta + \mathbf{S}_\gamma + \mathbf{S}_\delta$  and antiferromagnetic  $\mathbf{L} = \mathbf{S}_\alpha - \mathbf{S}_\beta + \mathbf{S}_\gamma - \mathbf{S}_\delta$  order parameters [15]. The change of  $\mathbf{M}$ ,  $\mathbf{L}$  and the exchange interactions between the copper ions due to temperature and magnetic field variations leads to a change in the Frenkel exciton parameters, thus providing optical access to the magnetic structure of  $\text{CuB}_2\text{O}_4$ . Below  $T < 5.7 \text{ K}$  the  $4b$  subsystem is in an incommensurate antiferromagnetic phase and when a magnetic field is applied along the  $a$  axis ( $\mathbf{B}_a$ ) it orients the copper spins perpendicular to  $\mathbf{B}_a$  in the basal  $ab$  plane along the  $b$  axis. This changes the antiferromagnetic order into the commensurate phase, where the magnetic order corresponds to the unit cell of  $\text{CuB}_2\text{O}_4$  along the  $c$  axis.

The contour plot in Fig. 2(a) provides an illustrative representation of the field evolution of the absorption  $\pi$  spectrum. In this measurement, the temperature was fixed at  $T = 5.5 \text{ K}$ . When the  $4b$  subsystem undergoes a phase transition, the spectrum displays a distinctly nonmonotonic character, which can be traced through the alteration of the Frenkel exciton absorption coefficients,  $\alpha_{A,B}$ , and the splitting,  $\Delta_F$ . Representative  $\pi$  spectra in each phase are depicted in Fig. 2(b). The dependences of  $\alpha_{A,B}$  on the magnetic field  $B_a$  measured at  $T = 5.5 \text{ K}$  are shown in Fig. 3(a). These dependences are strongly nonmonotonic. The abrupt jump occurs at  $B_a = 0.78 \text{ T}$  and two bends are located at 1.13 T and 1.57 T for both  $\alpha_A$  and  $\alpha_B$ . The splitting  $\Delta_F$  between lines A and B in the presence of an external magnetic field is given by the zero-field splitting  $\Delta^\zeta$  and some differences in Zeeman splitting of the A and B lines [32]. The parameters  $\alpha_B/\alpha_A$  and  $\Delta_F$  in dependence on  $B_a$  show three peculiarities at the same fields as  $\alpha_{A,B}$  marked by the arrows in Figs. 3(b) and 3(c). Also the width of the A and B exciton lines show three peculiarities at the same fields; see Fig. 4(a). Since the measured Frenkel excitons are related to the  $4b$  subsystem, we can definitely interpret them as the phase transitions within this subsystem. The sharp change of these parameters at  $B_a = 0.78 \text{ T}$  is a clear sign of a first order phase transition, whereas the smooth change at 1.13 T is a sign of a second order transition. A second order phase transition takes place also at 1.57 T.

Interestingly, the integral intensity of the A exciton line ( $I_A$ ) has the opposite dependence on magnetic field compared to that of the B line ( $I_B$ ), see Fig. 4(b), while the integral intensity of the entire spectrum evaluated as  $I_A + I_B$ , which is shown by a blue line, is independent of magnetic field. It is evident that the absorption intensities are redistributed between the A and B lines when the magnetic phases transition occurs.

Similar peculiarities in the temperature evolution of the  $\pi$  spectrum and of the Frenkel exciton parameters are observed in a magnetic field of  $B_a = 0.4 \text{ T}$ ; see Figs. 2(c), 2(d) and Figs. 3(d)–3(f). The abrupt jump in the  $\alpha_{A,B}$  temperature dependence at  $T = 5.6 \text{ K}$  confirms a first order transition, while the bend at 7.6 K is typical for a second order transition. At the same temperatures, phase transitions are seen for the  $\alpha_B/\alpha_A$  and  $\Delta_F$  dependences. These results demonstrate that the Frenkel exciton is a sensitive tool for monitoring magnetic-field- and temperature-induced phase transitions, which are selective to the magnetic subsystems, in our case to the  $4b$  subsystem. In the following, we reconstruct the detailed phase diagram and compare it to the magnetic data for magnetic phase identification.

### B. Magnetic field–temperature phase diagram for $\mathbf{B}_a \parallel a$

The full magnetic phase diagram in the  $\mathbf{B}_a$ - $T$  space based on the change of  $\Delta_F$  is shown in Fig. 5(a). The dashed lines highlight the values of  $\mathbf{B}_a$  and  $T$  where the peculiarities of  $\Delta_F$  and  $\alpha_B/\alpha_A$  occur. They form the boundaries between the magnetic phases of the  $\text{Cu}^{2+}$  ions in the  $\mathbf{B}_a$ - $T$  space. The evaluation of these phase boundaries is shown in Fig. 5(b), where the blue symbols correspond to discontinuous changes and the red symbols to smooth bends of  $\Delta_F$  and  $\alpha_B/\alpha_A$ . We found in experiment that the abrupt jumps exhibit a hysteresis behavior, as shown in Fig. 5(d). Such behavior is typical for a first order phase transition. For a second order phase transition, a smooth change of parameters without abrupt jumps and/or hysteresis is expected. This is what we find for the phase boundaries shown by the red symbols in Fig. 5(b). The phase boundaries and the order of phase transitions are in good agreement with the magnetic susceptibility measurements from Ref. [17], shown by the green lines in Fig. 5(b).

Comparing our data with those from Ref. [17], we identify in the presented parameter ranges of  $4 \text{ K} < T < 10 \text{ K}$  and  $0 \text{ T} < B_a < 2 \text{ T}$  the commensurate phase ( $C_1$ ) with a weak ferromagnetic moment and two incommensurate phases ( $\text{IC}_1$  and  $\text{IC}_2$ ). The phase transitions from the  $\text{IC}_2$  to  $\text{IC}_1$  and from  $\text{IC}_1$  to  $C_1$  phases are of the first order type [blue symbols in Fig. 5(b)], indicating that the  $\text{Cu}^{2+}$  ions experience a spontaneous spin flop. The amplitude of the jump for the transition from  $\text{IC}_1$  to  $C_1$  decreases with decreasing temperature, turning into a second order type transition to C-IC at 6.7 K. The phase boundary between C-IC and  $C_1$  is observed only in the change of the  $\alpha_B/\alpha_A$  parameter. Note that the phase transition between C-IC and  $C_1$ , shown by the open red circles in Fig. 5(b), had not been observed in the magnetic measurements in Ref. [17]. However, this transition had been detected in thermal conductivity measurements and assigned to the coexistence of commensurate and incommensurate antiferromagnetic phases [18].

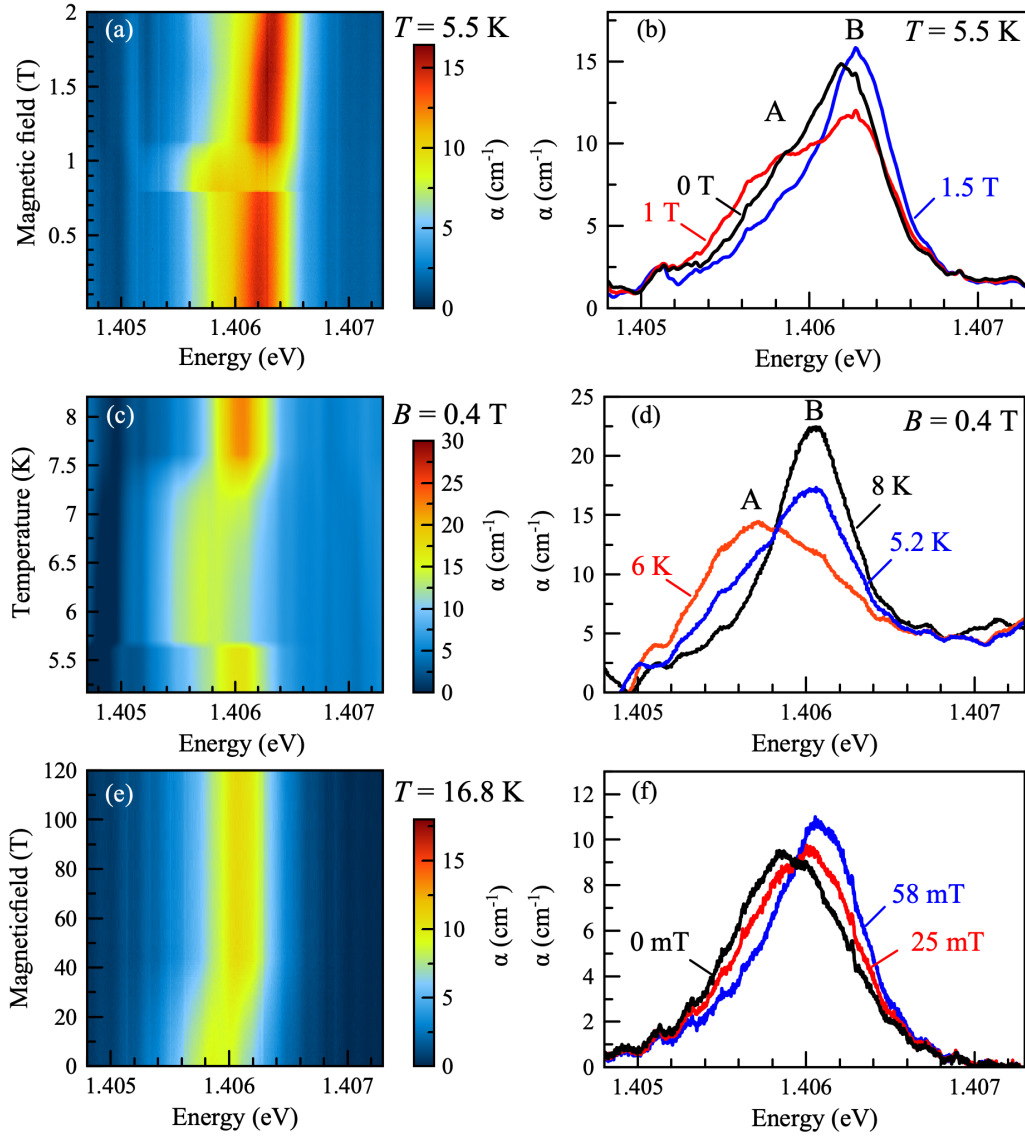


FIG. 2. Evolution of the absorption  $\pi$  spectrum of  $\text{CuB}_2\text{O}_4$  of the Frenkel exciton in different temperatures and magnetic fields ( $\mathbf{B}_a \parallel a$ ). Panels (a), (c), and (e) are contour plots in which the absorption amplitude is represented by color. In panel (a), the temperature was maintained at a constant value of  $T = 5.5$  K while the magnetic field was increased. (b) Absorption  $\pi$  spectra in the  $\text{IC}_2$  (0 T),  $\text{IC}_1$  (1 T), and C-IC (1.5 T) phases. In panel (c), the magnetic field was maintained at a fixed value of  $B = 0.4$  T while the temperature was scanned in the upward direction in steps of 0.1 K. The temperature change rate between the measurement of two adjacent spectra was less than 0.1 K/min. Additionally the temperature was maintained at each data point for a minimum of 10 min. This waiting period ensured a stable temperature of the sample within the cryostat. (d) Absorption  $\pi$  spectra in the  $\text{IC}_2$  (5.2 K),  $\text{IC}_1$  (6 K), and  $\text{C}_1$  (8 K) phases. In panel (e), the temperature was fixed at  $T = 16.8$  K while the magnetic field was scanned in an upward direction. (f) Absorption  $\pi$  spectra in the  $\text{C}_0^*$  (0 mT),  $\text{C}_0$  (25 mT), and  $\text{C}_1$  (58 mT) phase region.

The phases  $\text{IC}_1$ ,  $\text{IC}_2$ , and C-IC converge at the critical point  $T_0$  with the coordinates  $T = 4.5$  K and  $B_a = 1.24$  T. The phases  $\text{IC}_1$ ,  $\text{C}_1$ , and C-IC converge at the critical point  $T_1$  with the coordinates  $T = 6.7$  K and  $B_a = 0.73$  T. It is stated in Ref. [17] that the phase transition boundary  $\text{IC}_1$ – $\text{IC}_2$  terminates at the critical point  $T_{\text{cp}} = 5.8$  K and  $B_a = 0.3$  T. However, our experimental data show that this boundary is extended beyond  $T_{\text{cp}}$  and approaches 0 T at 5.74 K, as shown by the open blue circles in Fig. 5(b). This illustrates that, for clarifying all details of the magnetic phase diagram, experimental data gained by various techniques are required.

The magnetic phase diagram at higher temperatures  $T > 7$  K and weak magnetic fields of  $B_a < 0.08$  T is shown in Fig. 5(c). We identify here three commensurate phases ( $\text{C}_0$ ,  $\text{C}_0^*$ , and  $\text{C}_1$ ) and one incommensurate noncollinear phase  $\text{IC}_1^*$ . The contour plot in Fig. 2(e) highlights the field evolution of the absorption  $\pi$  spectrum at  $T = 16.8$  K, which reveals the distinct transitions between the different magnetic phases. Absorption  $\pi$  spectra in the  $\text{C}_0^*$  (0 mT),  $\text{C}_0$  (25 mT), and  $\text{C}_1$  (58 mT) phase region are shown in Fig. 2(f). The transitions between these phases have second order character. In the antiferromagnetic commensurate phase  $\text{C}_0^*$ , in weak magnetic

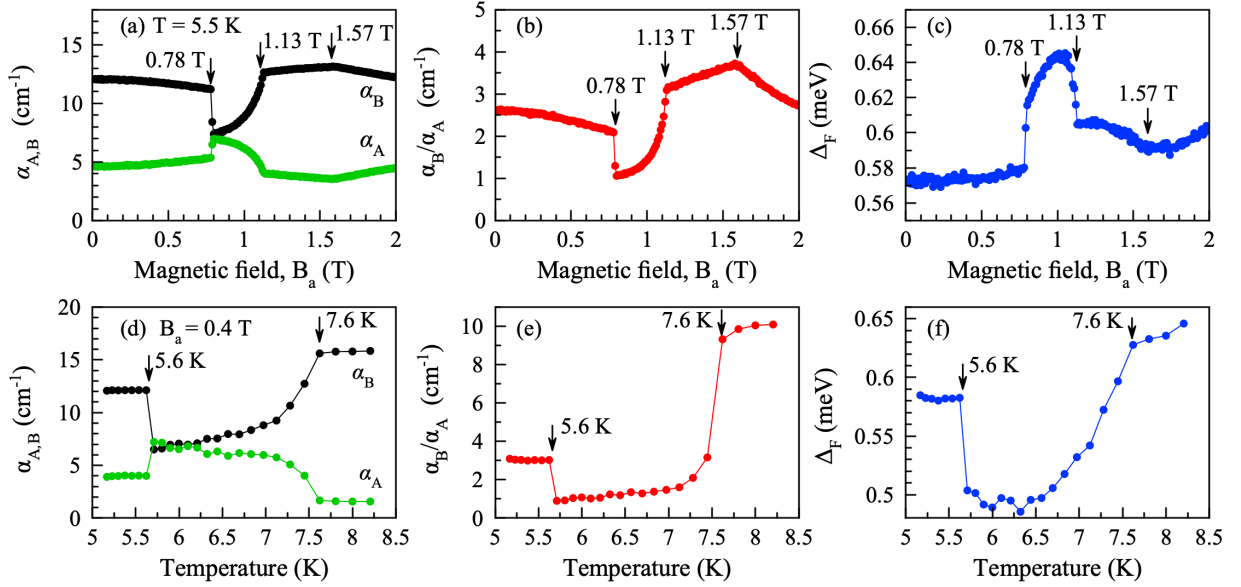


FIG. 3. Magnetic field and temperature dependences of the Frenkel exciton parameters at  $T = 5.5$  K or  $B_a = 0.4$  T. Magnetic field dependences ( $\mathbf{B}_a \parallel a$ ) of the (a) amplitudes of the A and B line absorption, (b) ratio  $\alpha_B/\alpha_A$ , and (c) excited state splitting  $\Delta_F$ . Arrows highlight peculiarities related to the phase transitions with the strength of  $B_a$ . Temperature dependences of the (d) absorption amplitudes, (e) ratio  $\alpha_B/\alpha_A$ , and (f)  $\Delta_F$ , all measured at  $B_a = 0.4$  T. The temperature in these measurements was increased from 5.2 to 8.2 K. Arrows depict the temperatures of phase transitions that are of the first (sharp changes) and the second (smooth changes) order, respectively.

fields the antiferromagnetic moment  $\mathbf{L}$  lies in the  $ab$  plane along the easy  $[110]$  axis and the ferromagnetic moment is  $\mathbf{M} = 0$ . Increasing the field  $B_a$  leads to the alignment of  $\mathbf{L}$  along the  $[010]$  axis with  $\mathbf{M} = 0$  forming the  $C_0$  phase. In higher  $B_a$ , the  $C_1$  antiferromagnetic commensurate phase exists with a weak ferromagnetic moment ( $\mathbf{L} \parallel \mathbf{b}$  and  $\mathbf{M} \neq 0$ ). We summarize the magnetic phase classification and Frenkel exciton parameters in Table I. One should note that, above the Néel temperature of 20 K, the  $\text{Cu}^{2+}$  ions are in a paramagnetic phase. In this phase and the chosen  $\mathbf{B}_a \parallel a$  geometry, the absorption at the  $4b$  Frenkel excitons is very low and it is not possible to accurately evaluate the exciton parameters.

### C. Magnetic field–temperature phase diagram for $\mathbf{B}_c \parallel c$

The magnetic field–temperature phase diagram is markedly different from that shown in Fig. 5 when the field is applied along the tetragonal  $c$  axis of  $\text{CuB}_2\text{O}_4$ .

This is caused by the collective reordering of the magnetic moments in the  $4b$  and  $8d$   $\text{Cu}^{2+}$  subsystems [15,17]. In zero magnetic field the spins of the  $4b$  subsystem lie within the  $ab$  easy plane, but the spins of the  $8d$  subsystem are directed predominantly along the tetragonal  $c$  axis. Such a predominantly orthogonal orientation of the spins in both subsystems makes coupling between them complicated [15,17]. In a field applied along the  $c$  axis the spins of the  $4b$  subsystem are subject to the perpendicular susceptibility. In contrast, the spins of the  $8d$  subsystem are subject to the parallel susceptibility. Both subsystems tend to be oriented along the  $c$  axis, but to a different degree because of their different magnetic susceptibilities. Above 9 K the  $8d$  subsystem is in a paramagnetic state, the coupling between the two subsystems is weak, and the phase diagram of  $\text{CuB}_2\text{O}_4$  is rather simple, as can be seen in Fig. 6(c). However, below 9 K the  $8d$  subsystem becomes partially ordered, so that the interaction between the two subsystems becomes

TABLE I. Parameters of the Frenkel excitons ( $\alpha_B/\alpha_A$  and  $\Delta_F$ ) in different spin phases for the magnetic field applied along the  $a$  axis ( $B_a$ ). C and IC denote the commensurate and incommensurate antiferromagnetic phases in the  $ab$  plane. The parameters are presented as ranges of the largest and lowest values detected for the respective magnetic phases. The last column gives the magnetic phase labels used in Ref. [17]. Note that the phases C-IC and  $C_1$  are not resolved in the magnetic measurements in Ref. [17], but are resolved in thermal conductivity measurements [18]. The antiferromagnetic C-IC phase is assigned to the coexistence of commensurate and incommensurate phases.

Magnetic phase	Order parameters	$\alpha_B/\alpha_A$	$\Delta_F$ (meV)	Magnetic phase [17]
$C_0$	$\mathbf{L} \parallel [010], \mathbf{M} = 0$	2.0 to 4.7	0.50 to 0.62	$\text{AF}_0$
$C_0^*$	$\mathbf{L} \parallel [110], \mathbf{M} = 0$	1.1 to 2.0	0.22 to 0.50	$\text{AF}_0^*$
$C_1$	$\mathbf{L} \parallel [010], \mathbf{M} \neq 0$	3.7 to 7.0	0.54 to 0.60	$\text{AF}_1$
C-IC		2.0 to 3.0	0.59 to 0.62	$\text{AF}_1$
$\text{IC}_1$	Helical order	0.3 to 3.1	0.39 to 0.68	$\text{P}_1$
$\text{IC}_1^*$	Elliptical order	0.9 to 1.9	0.39 to 0.48	$\text{P}_1$
$\text{IC}_2$	Helical order	1.5 to 2.5	0.56 to 0.59	$\text{P}_2$

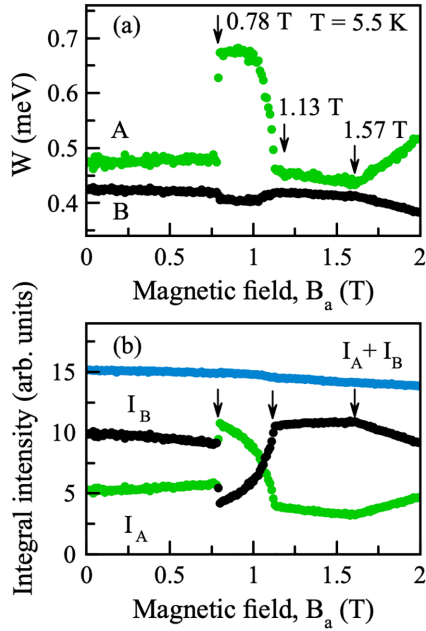


FIG. 4. Magnetic field dependences of the Frenkel exciton parameters at  $T = 5.5$  K. (a)  $W_A$  and  $W_B$  dependences on  $B_a$ . Arrows mark the field strengths of the phase transitions. (b)  $I_A$  (green) and  $I_B$  (black) integral intensities of the A and B lines. The total intensity of both lines ( $I_A + I_B$ ) is given by the blue symbols.

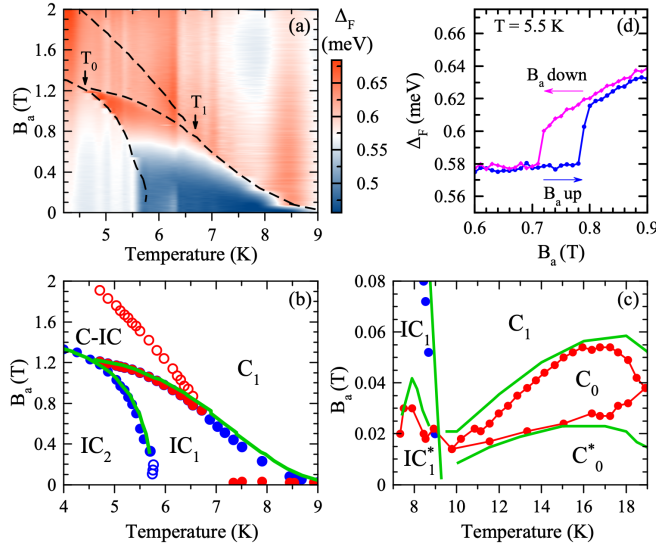


FIG. 5. Magnetic phase diagrams of  $\text{CuB}_2\text{O}_4$  measured for  $\mathbf{B}_a \parallel a$ . (a) Color-coded dependence of the splitting  $\Delta_F$  on temperature  $T$  and magnetic field  $B_a$ . Dashed lines show the phase boundaries. The critical points  $T_0$  and  $T_1$ , where several phases converge, are highlighted. (b), (c) Boundaries between magnetic phases obtained from  $\Delta_F$  and  $\alpha_B/\alpha_A$  for  $4 \text{ K} < T < 10 \text{ K}$  (b) and for  $7 \text{ K} < T < 19 \text{ K}$  (c). Symbols are the experimental data and green lines are data of the magnetic moment measurements from Ref. [17]. Open symbols highlight the optically detected phase transitions. Symbols of blue and red colors encode the first and second order types of phase transitions, respectively. C and IC with indices denote the commensurate and incommensurate antiferromagnetic phases, respectively. A detailed definition of the indices can be found in the text and in Table I. (d) Hysteresis in the  $\Delta_F$  dependence on  $B_a$ , measured at  $T = 5.5$  K.

important and consequently the phase diagram becomes more complicated.

The experimental data for the magnetic phase diagram for  $\mathbf{B}_c \parallel c$  are shown in Fig. 6. The color coded contour plot of  $\Delta_F$  as a function of  $T$  and  $B_c$  is presented in Fig. 6(a) for  $5 \text{ K} < T < 15 \text{ K}$  and  $0 \text{ T} < B_c < 1.6 \text{ T}$ . The black dashed lines highlight the phase transition boundaries, serving as guides to the eye. Their evaluation is shown in Fig. 6(b) by the red circles. All phase transitions are of the second order type and show no abrupt change of  $\Delta_F$  and/or hysteresis behavior.

In total seven phases are recognized:  $\text{IC}_1^c$ ,  $\text{IC}_2^c$ , and  $\text{IC}_3^c$ , which are incommensurate antiferromagnetic phases, and  $\text{C}_0^c$ ,  $\text{C}_1^c$ , and  $\text{C}_U^c$ , which are commensurate antiferromagnetic phases. The previous magnetic susceptibility measurements [17] had led to the conclusion that these phases originate from partial ordering of the  $8d$  copper spins below 9 K and the interaction between both copper subsystems.

Based on Ref. [17], below  $T = 7 \text{ K}$  and  $B_c < 0.2 \text{ T}$ , the copper spins in the  $8d$  subsystem have an antiferromagnetic moment along the  $c$  axis, forming the cone incommensurate phase  $\text{IC}_1^c$ . It was found that an increase of  $B_c$  leads to the incommensurate phase  $\text{IC}_2^c$ , where the spins of the  $4b$  subsystems become slightly tilted out of the  $ab$  plane due to the relevant magnetic susceptibility along the  $c$  axis. For  $B_c > 0.3 \text{ T}$ , the  $\text{IC}_3^c$  phase was identified. We see similar boundaries and phases in the experimental data obtained for the magnetic phase diagram shown in Fig. 6(b). When the temperature is increased above  $T = 9 \text{ K}$ , the spin system undergoes the transition from the  $\text{IC}_3^c$  phase to the commensurate phase  $\text{C}_1^c$  with a weak ferromagnetic moment for  $B_c > 0.4 \text{ T}$  and, for  $B_c < 0.4 \text{ T}$ , the commensurate antiferromagnetic phase  $\text{C}_0^c$  without a ferromagnetic moment was found [34].

The phase boundaries obtained from measurements of the magnetic moment [17] are shown by the green lines in Fig. 6(b). Comparing these results with the results of the optical absorption measurements, we see similar boundaries and phases detected only optically, but also highlights of the phase  $\text{C}_U^c$  at  $B_c > 1 \text{ T}$  at 9 K, in which we suppose that commensurate and incommensurate phases coexist. Additionally, we detect a phase ( $\text{C}_0^{c*}$ ) at  $B_c < 0.08 \text{ T}$  of unknown origin. The large difference to Ref. [17] is that the magnetic moment data show the boundary between  $\text{IC}_3^c$  and  $\text{C}_1^c$  at larger  $B_c$  up to 6.5 T, as plotted in Fig. 6(c). We can trace this boundary only up to  $B_c = 1 \text{ T}$  by detection of the Frenkel excitons' parameters in the  $4b$  subsystem. This limitation is related to the complex Davydov-Zeeman splitting at  $B_c > 1.4 \text{ T}$ , as shown in detail in Ref. [32]. In this regime, the parameters of the Frenkel excitons are mostly determined by the external magnetic field and become weakly sensitive to the magnetic interactions between the copper spins.

#### IV. CONCLUSIONS

We have shown in this paper that the parameters of the Frenkel excitons in the multiferroic  $\text{CuB}_2\text{O}_4$ , measured at cryogenic temperatures and in magnetic fields below 2 T, are sensitive to magnetic phase transitions. The Frenkel excitons related to the lowest in photon energy transition, which belongs to the  $\text{Cu}^{2+}$  ions in the  $4b$  subsystem, have been

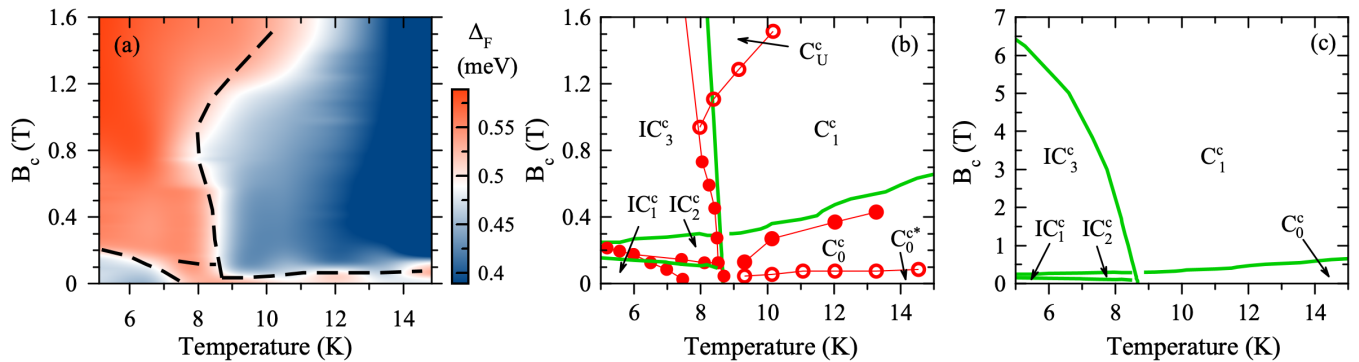


FIG. 6. Magnetic phase diagrams of CuB<sub>2</sub>O<sub>4</sub> measured for  $\mathbf{B}_c \parallel c$ . (a) Color-coded  $\Delta_F$  dependence on temperature and  $B_c$ . Dashed lines show the phase boundaries. (b) Measured phase boundaries are shown by the circles, where the open circles are for the transitions that have not been observed in Ref. [17]. Green lines are the results of the magnetic measurements of Ref. [17]. Red color of the symbols corresponds to a second order phase transition. C and IC with indices indicate the commensurate and incommensurate antiferromagnetic phases. Upper index “c” defines the change of the order parameters along the tetragonal  $c$  axis in the  $4b$  subsystem. (c) Phase boundaries from the magnetic measurements of Ref. [17] shown for  $B_c$  up to 7 T.

detected. The absorption amplitudes of the two exciton lines, their ratio, and their exchange splitting show clear changes, when the  $4b$  spin system is transformed between different magnetic phases. This provides a powerful tool for optical detection of the magnetic phase transitions and magnetic phases. Here it is used to measure the magnetic phase diagrams in CuB<sub>2</sub>O<sub>4</sub> for two different orientations of the magnetic field, along and perpendicular to the crystallographic  $c$  axis. The comparison of our results obtained from spectroscopic measurements of the  $4b$  subsystem with the recently published magnetic data that reflect the magnetic properties of both Cu<sup>2+</sup> subsystems [17,18] shows that the two types of phase diagrams coincide in their main features, but there are also differences. We detect a few phase transitions that had not been seen in magnetic measurements. Also, we show that the boundary between the IC<sub>1</sub>–IC<sub>2</sub> phases is not terminated at the critical point  $T_{cp} = 5.8$  K and  $B_a = 0.3$  T, but goes beyond  $T_{cp}$  and approaches 0 T at 5.74 K. Therefore, for clarifying all

details of the magnetic phase diagram, experimental data gained by different techniques are required. Optical techniques, in which the Frenkel exciton parameters can be determined, give direct access to the magnetic structure of particular subsystems in complex materials with several nonequivalent magnetic subsystems. This opens up opportunities for the optical study of magnetic structures in magnetic and multiferroic materials.

## ACKNOWLEDGMENTS

We are grateful to A. I. Pankrats for providing us with the magnetization data for comparison with our data and thank A. R. Nurmukhametov and M. V. Eremin for fruitful discussions. We acknowledge the financial support by the Deutsche Forschungsgemeinschaft through the Collaborative Research Center TRR142 (Project A11).

- 
- [1] M. Fiebig, Revival of the magnetoelectric effect, *J. Phys. D: Appl. Phys.* **38**, R123 (2005).
- [2] W. Eerenstein, N. D. Mathur, and J. F. Scott, Multiferroic and magnetoelectric materials, *Nature (London)* **442**, 759 (2006).
- [3] J. Wang, J. B. Neaton, H. Zheng, V. Nagarajan, S. B. Ogale, B. Liu, D. Viehland, V. Vaithyanathan, D. G. Schlom, U. V. Waghmare, N. A. Spaldin, K. M. Rabe, M. Wuttig, and R. Ramesh, Epitaxial BiFeO<sub>3</sub> multiferroic thin film heterostructures, *Science* **299**, 1719 (2003).
- [4] Y. Tokura, Sh. Seki, and N. Nagaosa, Multiferroics of spin origin, *Rep. Prog. Phys.* **77**, 076501 (2014).
- [5] M. Fiebig, T. Lottermoser, D. Meier, and M. Trassin, The evolution of multiferroics, *Nat. Rev. Mater.* **1**, 16046 (2016).
- [6] N. A. Spaldin, Multiferroics beyond electric-field control of magnetism, *Proc. R. Soc. A* **476**, 20190542 (2020).
- [7] B. Jana, K. Ghosh, K. Rudrapal, P. Gaur, P. K. Shihabudeen, and A. Roy Chaudhuri, Recent progress in flexible multiferroics, *Front. Phys.* **9**, 822005 (2022).
- [8] R. V. Pisarev, Broken symmetries and optical phenomena in crystals, *Ferroelectrics* **183**, 39 (1996).
- [9] R. V. Pisarev, Crystal optics of magnetoelectrics, *Ferroelectrics* **162**, 191 (1994).
- [10] R. Gupta and R. K. Kotnala, A review on current status and mechanisms of room-temperature magnetoelectric coupling in multiferroics for device applications, *J. Mater. Sci.* **57**, 12710 (2022).
- [11] A. Cano, D. Meier, and M. Trassin, *Multiferroics* (De Gruyter, Berlin/Boston, 2021).
- [12] G. A. Petrakovskii, A. D. Balaev, and A. M. Vorotynov, Magnetic susceptibility and magnetic-field behavior of CuB<sub>2</sub>O<sub>4</sub> copper metaborate, *Phys. Solid State* **42**, 321 (2000).
- [13] T. Fujita, Y. Fujimoto, S. Mitsudo, T. Idehara, K. Inoue, J. Kishine, Y. Kousaka, S. Yano, J. Akimitsu, and M. Motokawa, High field ESR measurements on the chiral spin system CuB<sub>2</sub>O<sub>4</sub>, *J. Phys.: Conf. Ser.* **51**, 111 (2006).

- [14] M. Boehm, B. Roessli, J. Schefer, B. Ouladdiaf, A. Amato, C. Baines, U. Staub, and G. A. Petrakovskii, A neutron scattering and  $\mu$ SR investigation of the magnetic phase transitions of  $\text{CuB}_2\text{O}_4$ , *Phys. B: Condens. Matter* **318**, 277 (2002).
- [15] M. Boehm, B. Roessli, J. Schefer, A. S. Wills, B. Ouladdiaf, E. Lelièvre-Berna, U. Staub, and G. A. Petrakovskii, Complex magnetic ground state of  $\text{CuB}_2\text{O}_4$ , *Phys. Rev. B* **68**, 024405 (2003).
- [16] Y. Kousaka, S. Yano, M. Nishi, K. Hirota, and J. Akimitsu, Magnetic soliton lattice in  $\text{CuB}_2\text{O}_4$  under an applied magnetic field, *J. Phys. Chem. Solids* **68**, 2170 (2007).
- [17] A. E. Petrova and A. I. Pankrats, Copper metaborate  $\text{CuB}_2\text{O}_4$  phase diagrams based on the results of measuring the magnetic moment, *JETP* **126**, 506 (2018).
- [18] T. Kawamata, N. Sugawara, S. M. Haidar, T. Adachi, T. Noji, K. Kudo, N. Kobayashi, Y. Fujii, H. Kikuchi, M. Chiba, G. A. Petrakovskii, M. A. Popov, L. N. Bezmaternykh, and Y. Koike, Thermal conductivity and magnetic phase diagram of  $\text{CuB}_2\text{O}_4$ , *J. Phys. Soc. Jpn.* **88**, 114708 (2019).
- [19] K. N. Boldyrev, R. V. Pisarev, L. N. Bezmaternykh, and M. N. Popova, Antiferromagnetic dichroism in a complex multisublattice magnetoelectric  $\text{CuB}_2\text{O}_4$ , *Phys. Rev. Lett.* **114**, 247210 (2015).
- [20] A. Molchanova and K. Boldyrev, High-resolution spectroscopy of low-temperature phase transitions in copper metaborate  $\text{CuB}_2\text{O}_4$ , *Opt. Spectrosc.* **127**, 33 (2019).
- [21] R. V. Pisarev, I. Sanger, G. A. Petrakovskii, and M. Fiebig, Magnetic-field induced second harmonic generation in  $\text{CuB}_2\text{O}_4$ , *Phys. Rev. Lett.* **93**, 037204 (2004).
- [22] J. Mund, D. R. Yakovlev, A. N. Poddubny, R. M. Dubrovin, M. Bayer, and R. V. Pisarev, Toroidal nonreciprocity of optical second harmonic generation, *Phys. Rev. B* **103**, L180410 (2021).
- [23] S. Toyoda, M. Fiebig, T. Arima, Y. Tokura, and N. Ogawa, Nonreciprocal second harmonic generation in a magnetoelectric material, *Sci. Adv.* **7**, eabe2793 (2021).
- [24] R. V. Pisarev and R. M. Dubrovin, Phonons, magnons, and excitons in the noncentrosymmetric magnetoelectric antiferromagnet  $\text{CuB}_2\text{O}_4$ , *JETP* **137**, 582 (2023).
- [25] M. Martinez-Ripoll, S. Martinez-Carrera, and S. Garcia-Blanco, The crystal structure of copper metaborate,  $\text{CuB}_2\text{O}_4$ , *Acta Cryst. B* **27**, 677 (1971).
- [26] D. Kudlacik, V. Yu. Ivanov, D. R. Yakovlev, V. F. Sapega, J. J. Schindler, J. Debus, M. Bayer, and R. V. Pisarev, Exciton and exciton-magnon photoluminescence in the antiferromagnet  $\text{CuB}_2\text{O}_4$ , *Phys. Rev. B* **102**, 035128 (2020).
- [27] S. Toyoda, N. Abe, and T. Arima, Gigantic directional asymmetry of luminescence in multiferroic  $\text{CuB}_2\text{O}_4$ , *Phys. Rev. B* **93**, 201109(R) (2016).
- [28] M. Saito, K. Taniguchi, and T.-H. Arima, Gigantic optical magnetoelectric effect in  $\text{CuB}_2\text{O}_4$ , *J. Phys. Soc. Jpn.* **77**, 013705 (2008).
- [29] S. Toyoda, N. Abe, S. Kimura, Y. H. Matsuda, T. Nomura, A. Ikeda, S. Takeyama, and T. Arima, One-way transparency of light in multiferroic  $\text{CuB}_2\text{O}_4$ , *Phys. Rev. Lett.* **115**, 267207 (2015).
- [30] A. I. Nikitchenko and R. V. Pisarev, Magnetic and antiferromagnetic nonreciprocity of light propagation in magnetoelectric  $\text{CuB}_2\text{O}_4$ , *Phys. Rev. B* **104**, 184108 (2021).
- [31] K. N. Boldyrev, A. D. Molchanova, A. R. Nurmukhametov, M. V. Eremin, R. V. Pisarev, and M. N. Popova, Nonreciprocity of optical absorption in the magnetoelectric antiferromagnet  $\text{CuB}_2\text{O}_4$ , *Magnetochemistry* **9**, 95 (2023).
- [32] N. E. Kopteva, D. Kudlacik, D. R. Yakovlev, M. V. Eremin, A. R. Nurmukhametov, M. Bayer, and R. V. Pisarev, Zeeman and Davydov splitting of Frenkel excitons in the antiferromagnet  $\text{CuB}_2\text{O}_4$ , *Phys. Rev. B* **105**, 024421 (2022).
- [33] G. A. Petrakovskii, K. A. Sablina, D. A. Velikanov, A. Vorotynov, N. V. Volkov, and A. F. Bovina, Synthesis and magnetic properties of copper metaborate single crystals,  $\text{CuB}_2\text{O}_4$ , *Crystallogr. Rep.* **45**, 853 (2000).
- [34] A. Pankrats, G. Petrakovskii, V. Tugarinov, K. Sablina, L. Bezmaternykh, R. Szymczak, M. Baran, B. Kundys, and A. Nabialek, Magnetic phase diagram of copper metaborate  $\text{CuB}_2\text{O}_4$  in magnetic field parallel to  $c$ -axis, *J. Magn. Magn. Mater.* **300**, e388 (2006).